Journal of Power Sources 250 (2014) 30–39

Contents lists available at ScienceDirect

Journal of Power Sources

journal homepage: www.elsevier.com/locate/jpowsour

Improved photocatalytic hydrogen production property over Ni/NiO/N–TiO_{2-x} heterojunction nanocomposite prepared by NH_3 plasma treatment

Shaozheng Hu [a,*], Fayun Li [a], Zhiping Fan [a], Jianzhou Gui [b]

[a] Institute of Eco-environmental Sciences, Liaoning Shihua University, Fushun 113001, PR China
[b] College of Chemistry and Materials Science, Liaoning Shihua University, Fushun 113001, Liaoning, PR China

HIGHLIGHTS

- Visible light responsive Ni/NiO/N–TiO_{2-x} nanocomposites were prepared by NH_3 plasma treatment.
- NH_3 plasma reduced partial NiO to metallic Ni, and formed high concentration of oxygen vacancies.
- Charge and structural compensation exist between TiO_2 and Ni species.
- Ni^0/Ni^{2+} ratio played a significantly important role on the photocatalytic H_2 production ability.

GRAPHICAL ABSTRACT

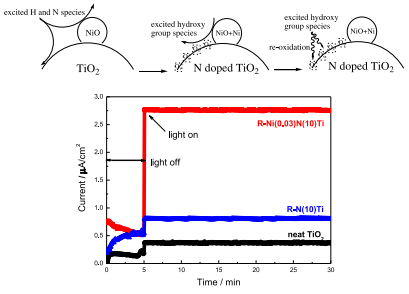

ARTICLE INFO

Article history:
Received 27 August 2013
Received in revised form
21 October 2013
Accepted 29 October 2013
Available online 7 November 2013

Keywords:
Plasma
Titaina
H_2 production
Heterojunction
Visible light

ABSTRACT

A series of visible light responsive Ni/NiO/N–TiO_{2-x} heterojunction nanocomposites are prepared by nonthermal NH_3 plasma treatment. X-ray diffraction, N_2 adsorption, UV–Vis spectroscopy, Electrochemical impedance spectroscopy, Photoluminescence, and X-ray photoelectron spectroscopy are used to characterize the prepared nanocomposites. Ni species deposition decreases the surface free energy of nanocomposites, reduce the thermodynamic driving force for particle growth, thus leading to the smaller particle sizes. NH_3 plasma treatment do not influence the crystal structure but shift its absorption edges to the visible light region, reduce partial NiO to metallic Ni, and form high concentration of oxygen vacancies. H_2 production performances on prepared TiO_2 nanocomposites are evaluated under visible light irradiation using CH_3OH as scavenger. The results indicate that Ni^0/Ni^{2+} ratio plays a significantly important role on the photocatalytic H_2 production ability. Adequate oxygen vacancies concentration can improve the visible light utilization, leading to an enhanced photocatalytic performance. The prepared R–Ni(0.03)N(10)Ti exhibited the highest H_2 production ability (1210 μmol h^{-1}) and apparent quantum yield (7.5%), which is 250 times higher than that of neat TiO_2. The possible mechanism is proposed.

1. Introduction

Hydrogen energy is a storable, clean, and environmentally friendly fuel, which is identified as an attractive candidate to replace the fossil fuels in the future. The scientists are much interested in finding ways to produce hydrogen from renewable energy sources such as solar and wind. Photocatalytic water splitting into hydrogen and oxygen by photocatalysts has been considered as a promising approach to resolve this problem since it was discovered by Honda and Fujishima in 1972 [1]. In order to produce hydrogen gas effectively, the conduction band of semiconductor should be more negative than that of H_2 production

* Corresponding author. Tel.: +86 24 23847473.
E-mail addresses: hushaozheng001@163.com, hushaozhenglnpu@163.com (S. Hu).

0378-7753/$ – see front matter © 2013 Elsevier B.V. All rights reserved.
http://dx.doi.org/10.1016/j.jpowsour.2013.10.132

potential and the valence band should be more positive than that of oxygen oxidation potential. It is counted by Osterloh et al. that over 130 inorganic materials and their derivatives were utilized as catalysts for water splitting in the past decades [2] Among them, TiO_2 has attracted extensive interest and considered to be most suitable for photocatalytic water splitting because of its low-cost, chemical inertness, opportune redox potential, non-toxicity, and long-term stability against photocorrosion and chemical corrosion [3]. However, the actual utilization of solar energy to produce hydrogen on TiO_2 is still difficult, due to the following shortcomings: 1) low solar light utilization, 2) short life time of photogenerated electrons, 3) fast backward reaction ($H_2 + 1/2\ O_2 \rightarrow H_2O$), and 4) large H_2 production overpotential [4]. Till now, many efforts have been devoted to conquer these shortcomings, including metal or nonmetal doping [5,6], combination with other semiconductors [7] or graphene [8], addition of sacrificial reagents [9], noble metals deposition [10], and formation of heterojunction [11].

N doping is considered to be the most effective approaches to enhance the visible light absorption since it was reported by Sato [12]. The doped N atoms narrowed the band gap of TiO_2 by mixing N 2p and O 2p states, therefore demonstrating the visible light activity. [13]. Deposition of noble metals has been proven to be very effective method to prolong life time of photogenerated electrons, thus was intensively investigated for photocatalytic H_2 production. The improved photocatalytic activity by noble metals deposition is due to the formation of Schottky barrier at the metal/semiconductor interface, which leads to the efficient charge separation [14]. Many noble metals, including Au, Pt, Ag, and Pd, were used for photocatalytic H_2 production [15–19]. The result is widely accepted that Pt/TiO_2 system exhibited the best H_2 production ability [17]. However, Pt is a rare and expensive noble metal which inhibits its practical application. Therefore, it is highly desirable to develop low-cost additives to replace Pt. More and more attentions have been focused on multicomponent photocatalysts. The intimate heterostructure which formed between components with different nanostructures can significantly improve the photogenerated charge separation and thereby promote the H_2 production ability [11,20,21]. Li et al. prepared $AgIn_5S_8/TiO_2$ heterojunction nanocomposite for H_2 production. They considered that the enhanced photoactivity can be ascribed to some $AgIn_5S_8$ nanoparticles closely contacting the TiO_2 nanoparticles to form heterojunction structure, which results in an efficient charge separation at the interface [11]. Brahimi et al. prepared $CuAlO_2/TiO_2$ heterojunction applied to visible light H_2 production [20]. They reported that ideal configuration $CuAlO_2/TiO_2$ heterojunction showed efficiency six times greater than that of $CuAlO_2$ under the same experimental conditions. Jang et al. prepared heterojunction photocatalyst $TiO_2/AgGaS_2$ for hydrogen production from water under visible light [21]. They suggested that the fabrication method was critical for the photocatalytic performance. This heterojunction configuration results in an efficient charge separation at the interface, followed by fast diffusion of photoelectrons generated in $AgGaS_2$ towards surrounding TiO_2, leading to high photocatalytic activity.

Recently, TiO_2 coupled with Ni or its derivatives is found to be an effective multicomponent photocatalyst [22–24]. NiO is a p-type semiconductor and easily forms heterojunctions with n-type TiO_2. Chen et al. prepared heterostructural photocatalyst comprising p-type NiO and n-type TiO_2 for degradation of methylene blue [22]. They considered the photoactivity enhancement is attributed to P–N junction and cocatalyst effects. Oros-Ruiz et al. reported the photocatalytic degradation of trimethoprim by metallic Ni nanoparticles supported on TiO_2–P25 [23]. The results show that the metallic Ni on the titania surface acts as a sink of electrons, promoting the formation of OH• radicals, thus increases the activity for the mineralization of trimethoprim. Yu et al. prepared $Ni(OH)_2$ cluster-modified TiO_2 nanocomposite for photocatalytic H_2 production [24]. They suggested that the function of metallic Ni is to help the charge separation and to act as cocatalyst for water reduction, thus enhancing the photocatalytic H_2-production activity. Considering both N and Ni are effective dopants to improve TiO_2 photocatalytic performance, combination of them should be a exciting modification method to improve TiO_2 photocatalytic performance. Moreover, Zhang et al. theoretically calculated the electronic structure, deformation charge density, dipole moment and optical property of N and Ni codoped anatase TiO_2 by density functional theory [25]. They found the codoping is helpful for enhancing the adsorption in visible-light region. However, only a few literature reported on N, Ni co-modified TiO_2 photocatalyst [26,27]. Zhang et al. prepare nitrogen and nickel co-doped TiO_2 for photocatalytic degradation of formaldehyde [26]. Hu et al. prepared composite photocatalyst, $N–TiO_2$ loaded with Ni_2O_3, and used for degradation of 2,4,6-trichlorophenol under visible light [27]. They suggested that the photocatalytic activity and stability of composite photocatalyst were much higher than that of catalyst modified with nitrogen or Ni_2O_3 alone. To our knowledge, there are few reports on the photocatalytic H_2 production over N, Ni co-modified TiO_2 photocatalyst.

Nonthermal plasma is composed of atoms, ions and electrons, which are much more reactive than their molecule precursors. Under plasma condition, a lot of reactions, which take place efficiently only at high temperature and pressure, can be initiated under mild conditions, thus is used frequently to prepare functional nanomaterials. Here, we report a convenient NH_3 plasma method to prepare visible light responsive $Ni/NiO/N–TiO_{2-x}$ heterojunction nanocomposites. The photocatalytic H_2 production ability of prepared catalysts were investigated under visible light.

2. Experimental

2.1. Preparation and characterization

In a typical experiment, 0.1 mol of $Ti(OC_4H_9)_4$ was dissolved in 100 mL ethanol to form solution A. Desired amount of $Ni(NO_3)_2{\cdot}6H_2O$ (molar ratio Ni/Ti = 0.01, 0.03, and 0.05) was dissolved in a mixture of 50 mL deionized water adjusted to pH = 3 with nitric acid and 50 mL ethanol to prepare solution B. Then, the solution A was added dropwise into the solution B under vigorous stirring at room temperature, and aged for 48 h to form the gel. The obtained gel was dried for 10 h at 80 °C, followed by milling and annealing at 500 °C for 2 h to remove the residual organic compounds (at a rate of 5 °C min^{-1}). The obtained product was denoted as Ni(x)Ti, where *x* stands for the molar ratio of Ni to Ti. For comparison, neat TiO_2 was prepared following the same procedure as in the synthesis of Ni(x)Ti but in the absence of nickelous nitrate.

A series of $Ni/NiO/N–TiO_{2-x}$ nanocomposites were conducted in a dielectric barrier discharge (DBD) reactor, consisting of a quartz tube and two electrodes. The high-voltage electrode was a stainless-steel rod (2.5 mm), which was installed in the axis of the quartz tube and connected to a high voltage supply. The grounding electrode was an aluminum foil which was wrapped around the quartz tube. For each run, 0.4 g Ni(*x*)Ti was charged into the quartz tube. At a constant NH_3 flow (40 ml min^{-1}), a high voltage of 9–11 kV was supplied by a plasma generator at an overall power input of 50 V × 0.4 A. The discharge frequency was fixed at 10 kHz, and the discharge was kept for 3–20 min. After discharge, the reactor was cooled down to room temperature. The obtained $Ni/NiO/N–TiO_{2-x}$ nanocomposites were denoted as R–Ni(*x*)N(*y*)Ti, where *y* stands for the plasma treated

time (min). For comparison, the mechanical mixing samples were prepared by mixing neat TiO_2 and NiO following the same procedure in the preparation of R–Ni(x)N(y)Ti. The obtained sample was denoted as M–Ni(x)N(y)Ti. When neat TiO_2 was used to replace Ni(x)Ti following the same procedure in the preparation of R–Ni(x)N(y)Ti, the product was denoted as R–N(y)Ti. When N_2 was used to replace NH_3 following the same procedure in the preparation of R–Ni(x)N(y)Ti, the product is denoted as Ni(x)N(y)Ti.

XRD patterns of the prepared TiO_2 samples were recorded on a Rigaku D/max-2400 instrument using Cu-Kα radiation ($\lambda = 1.54$ Å). UV–Vis spectroscopy measurement was carried out on a Jasco V-550 spectrophotometer, using $BaSO_4$ as the reference sample. The zeta-potential of the catalyst was measured at room temperature on Zetasizer Nano S90 (Malvern Instruments). The pH was adjusted by dropwise addition of dilute HCl or NaOH solution. Photoluminescence (PL) spectra were measured at room temperature with a fluorospectrophotometer (FP-6300) using an Xe lamp as excitation source. XPS measurements were conducted on a Thermo Escalab 250 XPS system with Al Kα radiation as the exciting source. The binding energies were calibrated by referencing the C 1s peak (284.6 eV) to reduce the sample charge effect. Working electrodes were prepared as follows: 0.3 g of sample was ground with 0.7 g of ethanol to make a slurry, then coated on an indium-tin oxide glass by the doctor blade method. Photocurrents were measured by electrochemical analyzer (CHI 618C Instruments) in a standard three electrode system which the prepared sample film was used as the working electrodes, a Pt flake as the counter electrode, and Ag/AgCl as the reference electrode. A 500 W Xe-lamp was used to irradiate the working electrode from the back side. A 1.0 M Na_2SO_4 solution was used as the electrolyte. Electrochemical impedance spectra (EIS) made from these as-made materials were measured via an EIS spectrometer (EC-Lab SP-150, BioLogic Science Instruments) in a three-electrode cell by applying 10 mV alternative signal versus the reference electrode (SCE) over the frequency range of 1 MHz–100 mHz. The cyclic voltammograms were measured in 0.1 M KCl solution containing 2.5 mM $K_3[Fe(CN)_6]/K_4[Fe(CN)_6]$ (1:1) as a redox probe with the scanning rate of 20 mV s^{-1} in the same three electrode cell as EIS measurement.

2.2. Photocatalytic reaction

The photocatalytic experiments were performed in an outer-irradiation and air-tight Pyrex glass reactor, connected to a water-cooling system. In a typical run, 1 g photocatalyst was suspended in 100 ml deionized water with methanol (10 vol.%, used as the hole scavenger) under stirring. Prior to the photocatalytic reaction, the suspension was purged with Ar gas for 20 min to get rid of O_2. A 110-W high-pressure sodium lamp with UV cutoff filter ($\lambda > 420$ nm) were used as light source. The photon flux measured using a radiometer (Model FZ-A, Photoelectric Instrument Factory Beijing Normal University, China) was determined to be 3.2×10^{-6} E·L^{-1} s^{-1}. A continuous magnetic stirrer was applied at the bottom of the reactor in order to keep the photocatalyst particles in suspension status during the whole experiment. The reaction products were analyzed on-line by thermal conductivity detectors on a micro-gas chromatography (Model Agilent P200 Series) equipped with a thermal conductivity detector (TCD) and a stainless steel column (2 m) packed with molecular sieves (5 A) at 323 K. Ar was used as the carrier gas at a flow rate of 20 cm^3 min^{-1}. All runs were conducted at ambient pressure and 30 °C. A schematic diagram of the photocatalytic H_2 evolution by water splitting process is shown in Fig. 1. The apparent quantum yield was determined as follows [28]:

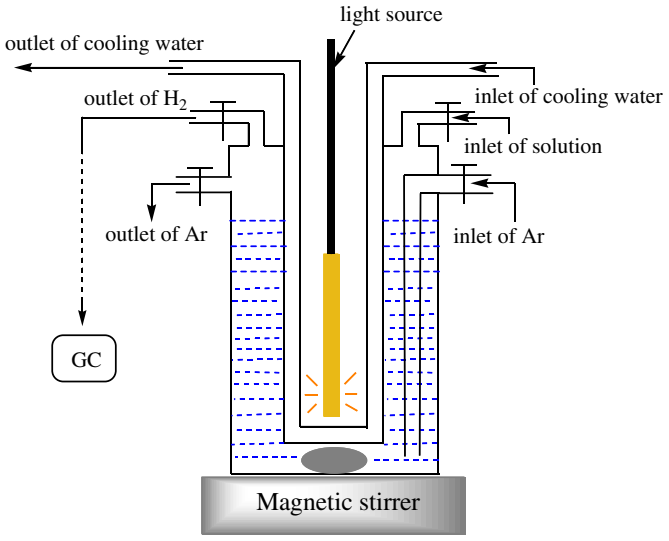

Fig. 1. Schematic diagram of the photocatalytic H_2 evolution by water splitting process.

$$\text{Quantum yield } (\%) = \frac{2 \times \text{number of evolved H2 molecules}}{\text{number of incident photons}} \times 100 \quad (1)$$

where the number of incident photons was determined by a chemical actinometry employing ammonium ferrioxalate [29].

3. Results and discussion

The XRD patterns of prepared TiO_2 catalysts are shown in Fig. 2. All samples exhibit the diffraction peaks of the anatase phase, indicating modification did not influence the crystal structure. The lattice parameters of prepared catalysts were measured according to the method of Shen [30]. The results shown in Table 1 indicate that the lattice parameters of all catalysts was unchanged along a- and b-axes, but c-axis parameter decreased obviously after NH_3 plasma treatment. This is probably due to that N atoms doped into

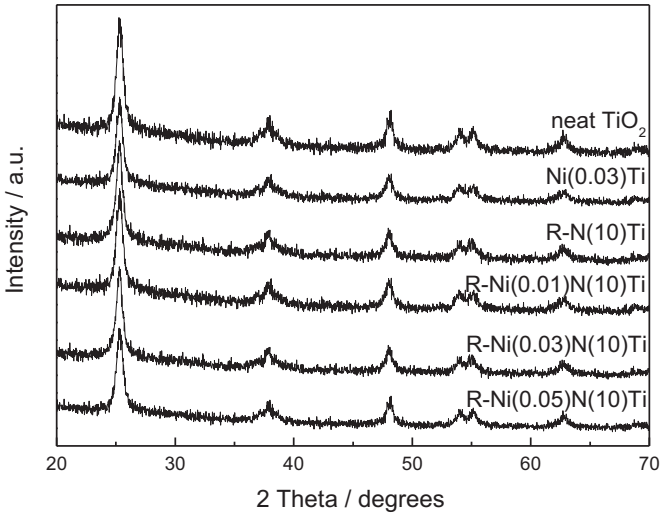

Fig. 2. XRD patterns of prepared TiO_2 based catalysts.

Table 1
Summary of physical properties of prepared TiO_2 samples.

Sample	[a] Size (nm)	S_{BET} ($m^2\ g^{-1}$)	Pore volume ($cm^3\ g^{-1}$)	Lattice parameters $a = b$, c (Å)
Neat TiO_2	18.2	88.9	0.27	0.37845, 0.95105
Ni(0.03)Ti	13.5	132.5	0.44	0.37841, 0.95136
R–N(10)Ti	17.8	91.3	0.29	0.37832, 0.94801
R–Ni(0.01)N(10)Ti	16.6	112.7	0.40	0.37838, 0.94778
R–Ni(0.03)N(10)Ti	13.3	133.9	0.42	0.37826, 0.94796
R–Ni(0.05)N(10)Ti	12.1	148.6	0.47	0.37851, 0.94771

[a] Particle size of prepared catalysts were calculated by their XRD patterns according to the Debye–Scherrer equation.

the TiO_2 lattice, leading to the decrease in the cell volume. Besides, in our previous report, we found that various excited hydrogen species were formed under NH_3 plasma condition, leading to the formation of high concentration of Ti^{3+} and oxygen vacancies [6]. Such oxygen vacancies caused the decrease in the cell volume. It is noted that the lattice parameters was unchanged for all the Ni contained TiO_2 nanocomposites compared with neat TiO_2, indicating Ni species was not doped into the lattice but separated from the phase. However, no Ni species crystalline phase was observed, which is probably due to that the amount of Ni is very small beyond the detection limit of this technique. Besides, the particle sizes of Ni contained TiO_2 nanocomposites decreased obviously compared with neat TiO_2 (Table 1). The higher Ni content, the smaller particle sizes of prepared nanocomposites. Kang et al. [31] and Pan et al. [32] prepared transition metal modified TiO_2 catalysts and found the similar phenomenon that the transition metal modification can suppress the crystal growth. It is known that the growth of small nanoparticle is dominated not by bulk ion transport but by surface process. Therefore, Ni species deposited on TiO_2 surface could decrease the surface free energy of nanocomposites, reduce the thermodynamic driving force for particle growth, thus leading to the smaller particle sizes. Generally, a catalyst with high specific surface area (S_{BET}) and big pore volume is significant to the enhancement of catalytic performance [33]. Neat TiO_2 and R–N(10)Ti showed the S_{BET} and pore volume lower than 90 $m^2\ g^{-1}$ and 0.3 $cm^3\ g^{-1}$ (Table 1). For Ni contained TiO_2 nanocomposites, the S_{BET} and pore volume increased obviously, which is consistent with the fact that smaller particle sizes should have a larger S_{BET} and pore volume [34]. The large S_{BET} and pore volume can promote the ability of adsorption, desorption, and diffusion of reactants and products, which is favorable to the catalytic performance [35].

To study the optical properties of prepared TiO_2 based catalysts, UV–Vis spectra were measured, as shown in Fig. 3. The absorption intensity starts to increase rapidly at 400 nm for neat TiO_2, corresponding to the intrinsic band gap absorption of anatase TiO_2. For Ni(x)Ti series catalysts (Fig. 3a), the small absorption shoulder around 400–500 nm were observed. Moreover, this absorption increased with increasing the Ni content. According to result of Irie [36], such absorption at ~450 nm is ascribed to the direct interfacial charge transfer from the valence band of TiO_2 to Ni^{2+}. Besides, the absorption bands did not shift, indicating the band gap energy is unchanged. In Fig. 3b, obvious red-shifts of the absorption bands were observed for NH_3 plasma treated TiO_2 catalysts, probably due to the electronic transition from the N 2p level, which is formed by incorporation of nitrogen atoms into the TiO_2 lattice, to the conduction band [37]. Such absorption band shift caused the decreased band gap energy, leading to the catalysts can be excited by visible light. Moreover, the broad absorptions in the whole visible light region were observed in the spectra of R–N(y)Ti catalysts. Abe et al. [38] treated TiO_2 catalyst by NH_3/Ar plasma and found the similar broad absorption. They suggested that such broad absorption is attributed to the presence of Ti^{3+}, which might be formed by plasma treatment. This broad absorption increased with increasing the plasma treated time, indicating the Ti^{3+} concentration increased. For R–Ni(x)N(y)Ti series catalysts (Fig. 3c), not only absorption shoulder around 400–500 nm but also red-shift of the absorption bands were observed simultaneously, implying their effective interfacial charge transfers and narrowed band gap energies. Besides, for mechanical mixing sample M-Ni(0.03)N(10)Ti, the absorption shoulder around 400–500 nm was sharply decreased, whereas a broad absorption at 600–800 nm which assigned to d–d transition of Ni^{2+} was observed [39]. This indicated that the interfacial charge transfer in M-Ni(0.03)N(10)Ti catalyst was much weaker than that of R–Ni(x)N(y)Ti series catalysts. Interestingly, the broad absorptions in the whole visible light region of R–Ni(x)N(y)Ti series catalysts decreased obviously compared with that of R–N(10)Ti, indicating the Ti^{3+} concentration decreased. The possible reason will be discussed later.

In order to further understand the interactions among chemical compositions of prepared nanocomposites and identify the chemical status of Ni element, the nanocomposites were characterized by XP spectra. Fig. 4 displays the XP spectra of prepared TiO_2 based catalysts in the region of Ti 2p (a), O 1s (b), N 1s (c), and Ni 2p (d). In Ti 2p region (Fig. 4a), both neat TiO_2 and Ni(0.03)Ti exhibited two peaks which could be assigned to Ti^{4+} $2p_{3/2}$ and Ti^{4+} $2p_{1/2}$ with the binding energy differences, $\Delta E = E(\text{Ti } 2p_{1/2}) - E(\text{Ti } 2p_{3/2})$, were around 5.7 eV [40]. After N_2 plasma treatment, Ni(0.03)N(10)Ti exhibited an obvious chemical shift to a lower binding energy compared with that of neat TiO_2, indicating a increase of electron density of Ti. This is probably due to that N atoms doped into TiO_2 lattice during N_2 plasma treatment. The electrons of N atoms may be partially transferred from N to Ti, due to the higher electronegativity of oxygen, leading to increased electron density. For R–Ni(0.03)N(10)Ti, a further chemical shift to lower binding energy was observed, which should be due to that the excited hydrogen species formed by NH_3 plasma condition can reduce partial Ti^{4+} to Ti^{3+}, leading to the lower effective positive charge of Ti. In Fig. 4b, the O 1s region is fitted with peaks corresponding to Ti–O bond from the TiO_2 lattice (530 eV) and O–H bond (532 eV). It is reported that oxygen from NiO, Ni hydroxides, and oxyhydroxides appear at 529.3, 531.1 and 530.8 eV, respectively [41]. Nevertheless, the associated oxygen signal was not observed. This is probably due to the low nickel concentration, leading to the oxygen signals are shielded. In Fig. 4c, the XP spectra of R–Ni(0.03)N(10)Ti in N 1s region were deconvoluted into three contributions. The peaks around 396.4 and 399.9 eV are attributed to formation of Ti–N bond and other surface N species such as N–N and N–O bond [42,43]. This result confirmed that N atoms doped into TiO_2 lattice in the formation of Ti–N bond. Li et al. [44] prepared N doped TiO_2 in NH_3/ethanol fluid under supercritical condition, and suggested that the N species located at 395.3 eV was attributed to the surface adsorbed NH_3 molecules. Therefore, the peak at 395.5 eV is attributed to the surface adsorbed NH_3 molecules. In Fig. 4d, Ni(0.03)N(10)Ti displays a Ni 2p peak around 856.6 eV, which is attributed to oxidized Ni (NiO) [45]. After NH_3 plasma treatment, another peak around 852.9 eV appeared, which should be due to the formation of metallic Ni [46]. It is known that NiO can be reduced to metallic Ni by H_2 at high temperature (800–1000 °C) [47,48]. Under plasma condition, electrons with high energy collide inelastically with NH_3 molecules and transfer their energy to the latter, which leads to the production of excited hydrogen species with significantly higher reduction ability than molecular hydrogen [49]. Those excited hydrogen species reduced not only Ti^{4+} but also Ni^{2+} to low valence.

According to the XPS data of prepared TiO_2 based catalysts, surface elemental compositions were calculated and shown in

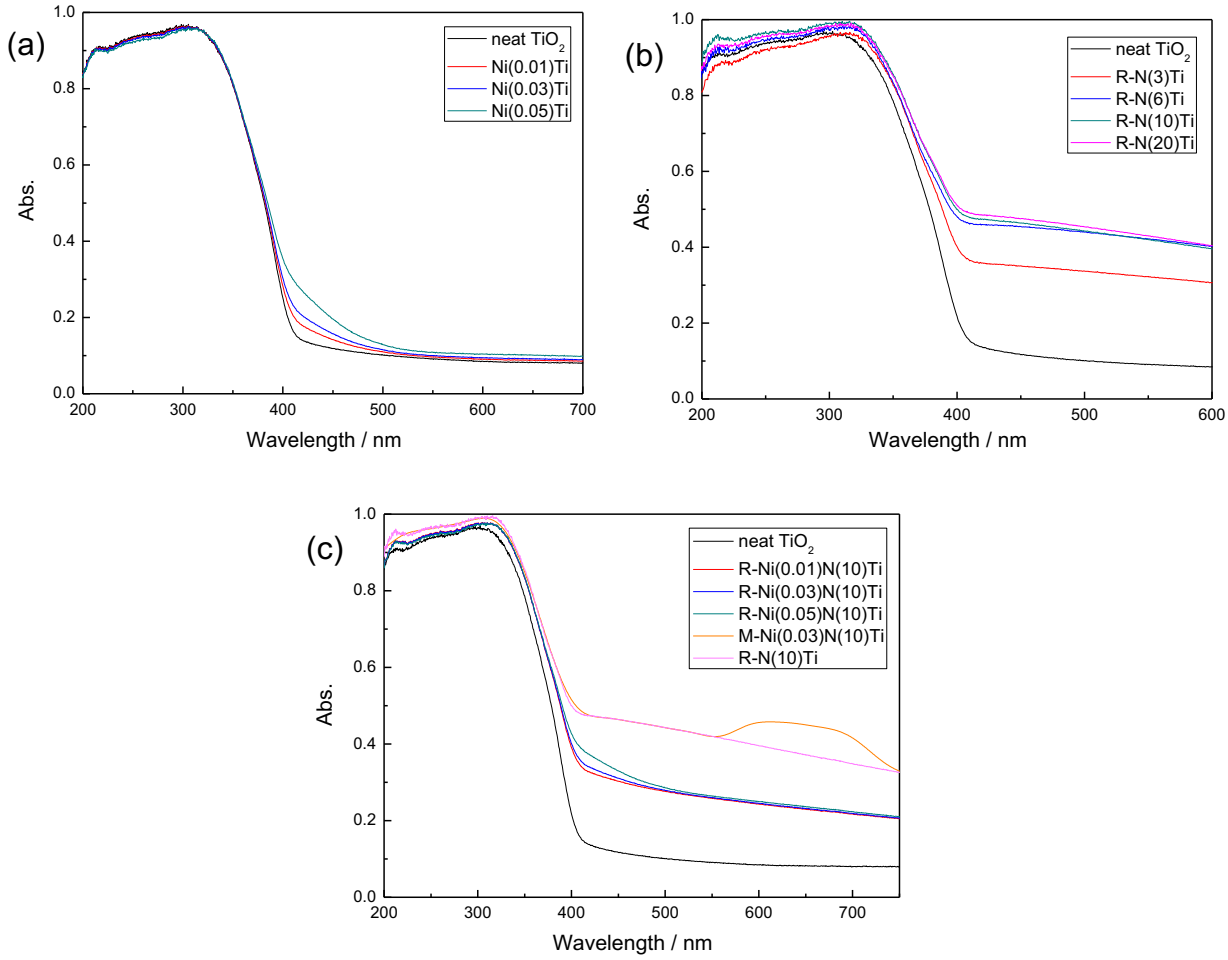

Fig. 3. UV–Vis diffuse reflectance spectra of prepared TiO_2 based catalysts.

Table 2. The O/Ti ratio of neat TiO_2 is exactly equal to 2. R–N(10)Ti exhibits a lower (O + N)/Ti ratio compared with neat TiO_2 (1.8). Liu et al. [50] suggested that oxygen vacancies existed when the (O + N)/Ti ratio was lower than 2.0. Therefore, it is deduced that NH_3 plasma treatment could introduce high concentration of oxygen vacancies in TiO_2 catalyst which is consistent with UV–Vis result. The (O + N)/Ti ratio of R–Ni(*x*)N(*y*)Ti series catalysts are higher than that of R–N(10)Ti. Furthermore, the higher Ni content in catalysts, the higher (O + N)/Ti ratio obtained. This result implies that Ni species deposited on TiO_2 surface could decrease the oxygen vacancies content effectively. However, for M-Ni(0.03)N(10)Ti, the (O + N)/Ti ratio is 1.8, indicating the preparation method influences the surface property of catalyst significantly. This result is interesting and the reason is not sure till now. We proposed the possible reason is that R–Ni(*x*)N(*y*)Ti series catalysts were prepared by wet chemical method, leading to their molecular spacing were much smaller than that prepared by mechanical mixing method (M-Ni(0.03)N(10)Ti). Under 9–11 kV high voltage plasma discharge treatment, strong interactions were formed between Ni species and TiO_2, leading to the formation of charge and structural compensation between them. Thus, R–Ni(*x*)N(*y*)Ti series catalysts show higher (O + N)/Ti ratio compared with R–N(10)Ti, whereas M-Ni(0.03)N(10)Ti is not. In order to confirm our point of view, the XPS analysis was measured again when the catalysts were preserved for a week (not shown here). The (O + N)/Ti ratio of R–N(10)Ti increases to 1.95 because the oxygen vacancies are unstable in air and easy to be oxidized. However, for R–Ni(*x*)N(*y*)Ti series catalysts, the (O + N)/Ti ratios are unchanged. Wu et al. [51] prepared Fe^{3+} doped TiO_2 with high oxygen vacancy concentrations and found that part of the Ti^{4+} ions changes their coordination number from 6 to 4 at high oxygen vacancy concentrations. They suggested that Fe^{3+} act as charge acceptors which are compensated by oxygen vacancies. Thus the oxygen vacancies were stable, and tetrahedrally coordinated Ti^{4+} were formed. Similarly, in this Ni/NiO/N–TiO_2 nanocomposite, charge compensation effect exists probably among compositions which stabilize the oxygen vacancy concentrations. Such compensated doping in TiO_2 can reduce the recombination centers which effectively accelerate the charge carriers' migration and enhance the photocatalytic activity [52,53]. The lattice N content (Ti–N) of R–N(10)Ti is 1.88 at.%. For Ni species deposited TiO_2 catalysts, the lattice N content decreases. The higher Ni content, the lower lattice N content. This is probably due to the cover of TiO_2 surface by Ni species which restrains the interaction between TiO_2 and excited nitrogen species. Ni content of Ni(0.03)Ti is 6.8 at.%, indicating Ni exists mainly on the TiO_2 surface. Metallic Ni and NiO are obtained in R–Ni(*x*)N(*y*)Ti series catalysts simultaneously. Whereas, for Ni(0.03)N(10)Ti, only NiO is observed with B.E. of 856.6 eV, indicating Ni^{2+} can not be reduced under N_2 plasma. The Ni^0/Ni^{2+} ratio for R–Ni(0.01)N(10)Ti, R–Ni(0.03)N(10)Ti, and R–Ni(0.05)N(10)Ti are 0.5, 0.66, and 0.33 respectively. This value is only 0.29 for mechanical mixing sample, M-Ni(0.03)N(10)Ti. This is possible due to that some interaction existed between NiO and TiO_2 in R–Ni(*x*)N(*y*)Ti series catalysts which cause the $Ni^{2+} \rightarrow Ni^0$ easier under NH_3 plasma condition than that of M-Ni(0.03)N(10)Ti.

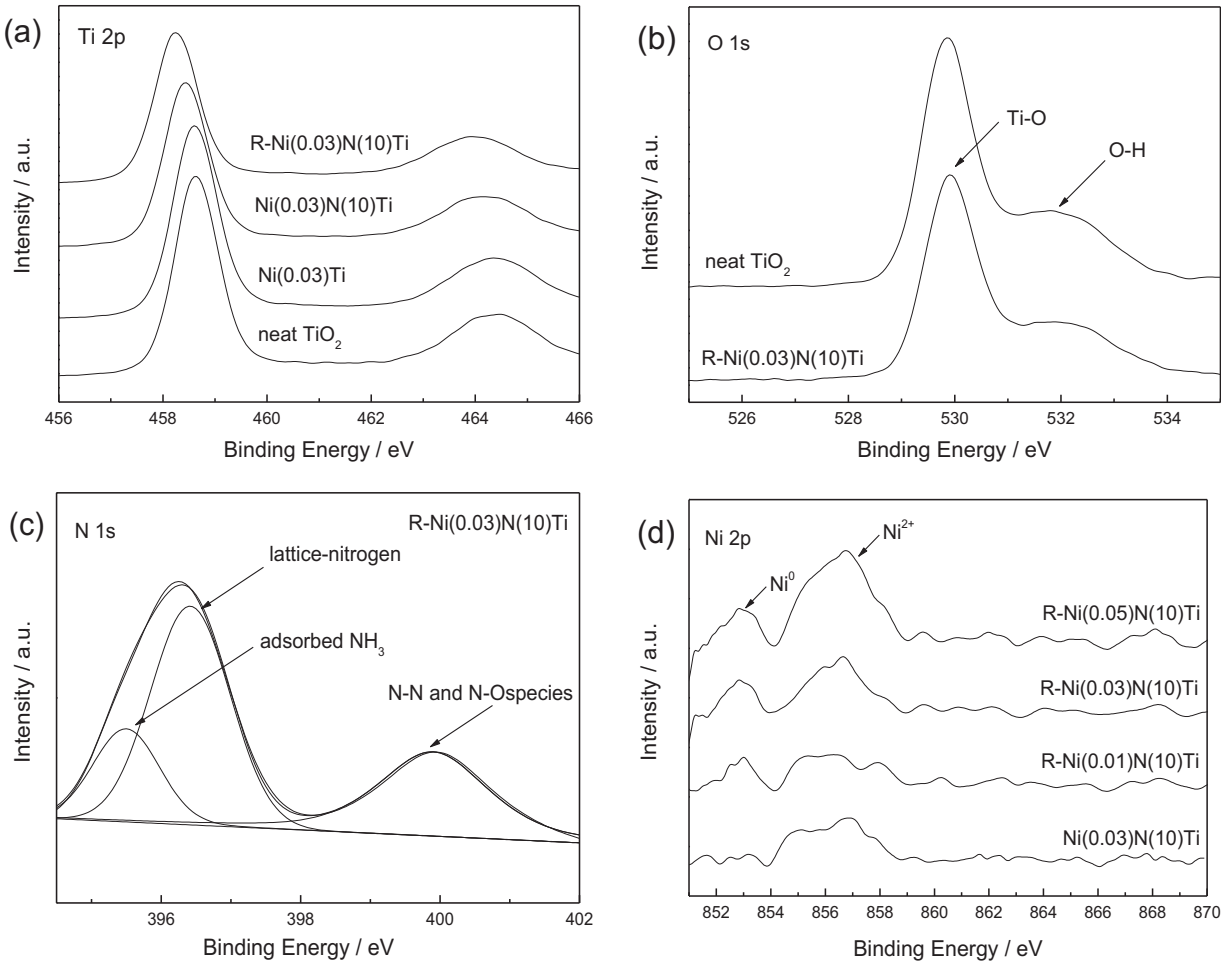

Fig. 4. XP spectra of prepared TiO_2 based catalysts in the region of Ti 2p (a), O 1s (b), N 1s (c), and Ni 2p (d).

Summarizes the obtained results above, we propose that the possible process is as follows (Fig. 5). For R–N(10)Ti, N doped into TiO_2 lattice under NH_3 plasma, and excited hydrogen species with high energy can reduce TiO_2 to produce high concentration of Ti^{3+}

Table 2
Surface elemental compositions of prepared TiO_2 based catalysts determined by XPS.

Sample	N		Ni		[a](O + N)/Ti
	B. E. (eV)	at.%	B. E. (eV)	at.%	
Neat TiO_2	–	–	–	–	2.0
Ni(0.03)Ti	–	–	856.6	6.8	2.02
R–N(10)Ti	395.5	0.7	–	–	1.8
	396.4	1.88			
	399.9	0.95			
Ni(0.03)N(10)Ti	396.4	1.6	856.6	6.6	1.98
	399.9	1.4			
R–Ni(0.01)N(10)Ti	395.5	0.6	852.9	0.7	1.89
	396.4	1.7	856.6	1.4	
	399.9	0.85			
R–Ni(0.03)N(10)Ti	395.5	0.52	852.9	2.7	1.91
	396.4	1.65	856.6	4.1	
	399.9	0.7			
R–Ni(0.05)N(10)Ti	395.5	0.41	852.9	2.5	1.93
	396.4	1.5	856.6	7.5	
	399.9	0.6			
M-Ni(0.03)N(10)Ti	395.5	0.7	852.9	0.7	1.8
	396.4	1.85	856.6	2.4	
	399.9	0.92			

[a] N represents the lattice N content with the binding energy of 396.4 eV.

and oxygen vacancies meanwhile. When NiO exists (R–Ni(x)N(y)Ti), the excited hydrogen species will reduce NiO to form metallic Ni and excited hydroxyl group species (Eq. (2)). Such excited hydroxyl group species can diffuse to TiO_2 surface easily because of the small molecular spacing, and re-oxidate partial Ti^{3+}, leading to the decreased oxygen vacancies concentration (Eq. (3)). The produced excited hydroxyl group species are consumed, which accelerates the NiO reduction, thus leading to a higher Ni^0/Ni^{2+} ratio. For mechanical mixing sample, such interaction between NiO and TiO_2 can not occur because of the wider molecular spacing. Therefore, R–Ni(x)N(y)Ti series catalysts exhibited higher Ni^0/Ni^{2+} ratio and lower oxygen vacancies concentrations.

$$H^* + NiO \longrightarrow Ni + OH^* \quad (2)$$

$$O_v + OH^* + Ti^{3+} \longrightarrow Ti^{4+}{-}O + H^* \quad (3)$$

During the recombination process of photo-induced charge carriers, a certain amount of chemical energy is released, following by transform to heat or light energy. The light energy is dissipated as radiation, which results in a luminescence emission of semiconductor, called the PL phenomenon. PL is a highly sensitive technique used to provide information on charge separation/recombination of photoinduced charged carriers [54]. In general, the lower PL intensity, the higher separation rates of photogenerated e^-/h^+ pairs, thus the higher the photocatalytic activity. Fig. 6 presents a comparison of PL spectra of prepared TiO_2 based

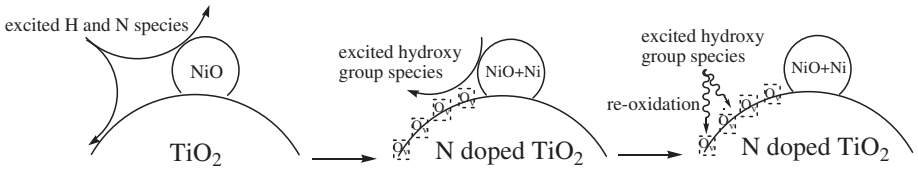

Fig. 5. The possible formation process of R–Ni(x)N(y)Ti series catalysts under NH_3 plasma.

catalysts. Five peaks located at 400, 430, 440, 452, and 470 nm were observed. The emission at 400 nm with band gap energy of 3.1 eV can be attributed to the free exciton, $O^{2-} \rightarrow Ti^{4+}$ charge–transfer transition. The emission at 430, 440, 452, and 470 nm should originate from the charge transfer transition of an oxygen vacancy trapped electron [55,56]. It could be found that all the prepared TiO_2 based catalysts exhibit obvious PL signal with similar curve shape, demonstrating that modification did not result in new PL phenomena, while the PL intensities of prepared catalysts were influenced. Ni(0.03)Ti exhibits a lower PL intensity compared with neat TiO_2, which confirms the charge transfer occurred between NiO and TiO_2, leading to the lower electron–hole recombination rate. This is consistent with the UV–Vis result (Fig. 3a). After NH_3 plasma treatment, R–Ni(x)N(y)Ti series catalysts display the further decreased PL intensities. Most of the electrons and holes recombine in nanoseconds. If scavengers or surface defects (such as oxygen vacancies) are present to trap the electrons or holes, the electron-hole recombination can be suppressed, leading to a photoluminescence quenching, such as R–Ni(x)N(y)Ti series catalysts. Whereas, the excess oxygen vacancies concentration act as recombination centers for excited electrons and holes, leading to the increased PL intensity for R–N(10)Ti compared with neat TiO_2. For mechanical mixing sample, the charge transfer and structural compensation can not occur because of the wider molecular spacing. Thus M-Ni(0.03)N(10)Ti exhibits higher electron-hole recombination rate than that of neat TiO_2, because of its excess oxygen vacancies concentration.

Electrochemical impedance spectroscopy (EIS) is a very useful tool to characterize the charge carrier migration, thus was used to further confirm the interfacial charge transfer effect of as-prepared TiO_2 nanocomposites. Fig. 7 shows the EIS Nyquist plots of the as-prepared TiO_2 catalysts under visible light irradiation. Obviously, R–Ni(0.03)N(10)Ti shows much decreased arc radius compared with R–N(10)Ti and neat TiO_2. The reduced arc radius indicates diminished resistance of working electrodes, suggesting a decrease in the solid state interface layer resistance and the charge transfer resistance across the solid–liquid junction on the surface by forming hybrid structures of TiO_2 with Ni species [57]. Since the radius of the arc on the EIS spectra reflects the migration rate occurring at the surface, it suggests that a more effective separation of photogenerated electron-hole pairs and a faster interfacial charge transfer occurs on R–Ni(0.03)N(10)Ti surface under this condition [58].

The outstanding carrier separation ability of R–Ni(0.03)N(10)Ti nanocomposite is confirmed by the photocurrent responses measurement (I–t curve, Fig. 8). Without doubt, almost no photocurrent was observed for neat TiO_2. The photocurrent value of R–Ni(0.03)N(10)Ti was ~3 times as high as that of R–N(10)Ti, which can be attributed to the intimate interaction existing on the TiO_2/Ni species interface, where photogenerated electrons and holes are efficiently separated, leading to the decreased photoinduced carrier recombination, corresponding to its enhanced photocurrent. Combination with above results, it is concluded that Ni species are in intimate contact with TiO_2 in R–Ni(0.03)N(10)Ti, leading to the formation of heterojunction. Such intimate heterostructure can significantly improve the photogenerated charge separation and thereby promote the photocatalytic efficiency [11,59,60]. Besides, the photocurrent responses did not decay with the increased illuminated time, indicating the prepared catalysts could provide stable quantity of electrons and holes during the irradiation. This hints that the prepared catalysts should exhibit the stable photocatalytic activities.

It is known that electrons and holes will be generated when TiO_2 is excited by light irradiation with the energy beyond band gap energy. The photogenerated holes will react with H_2O molecules to form H^+ and •OH. The photogenerated electrons from the conduction band attack H^+ to form an H atom. Finally, two H atoms

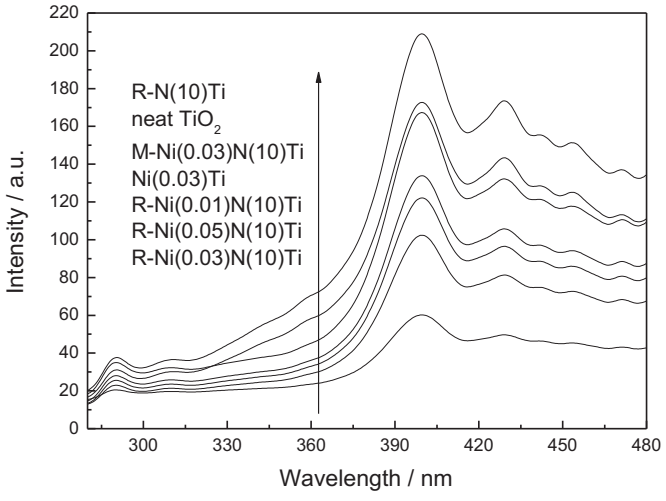

Fig. 6. Photoluminescence emission spectra of prepared TiO_2 based catalysts.

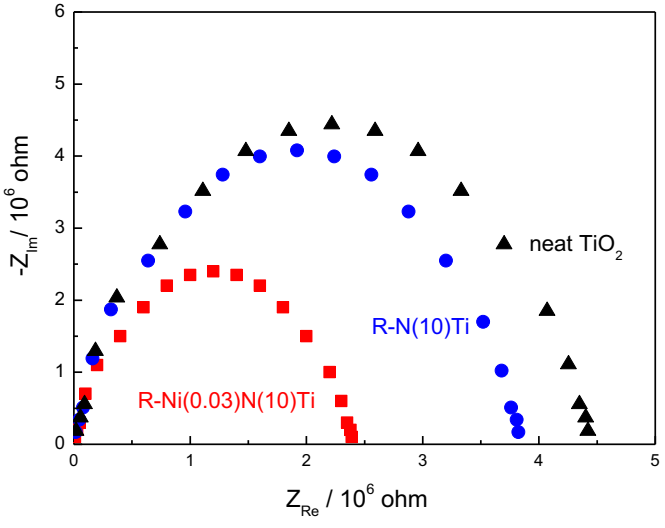

Fig. 7. EIS spectra of neat TiO_2, R–N(10)Ti, and R–Ni(0.03)N(10)Ti.

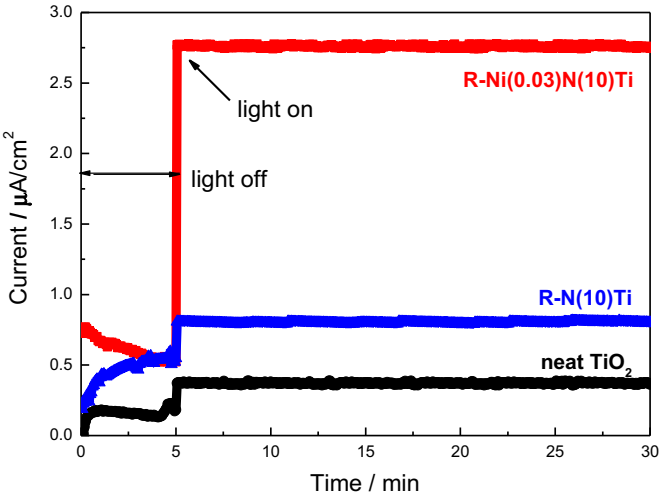

Fig. 8. The photocurrent responses of neat TiO_2, R–N(10)Ti, and R–Ni(0.03)N(10)Ti in 1.0 M Na_2SO_4 solution under visible light.

combine with each other to form a H_2 molecule (Eq. (4) ~ Eq. (6)). In order to accelerate the decomposition of H_2O to H^+ and •OH (Eq. (4)), CH_3OH is used as the sacrificial agent in our work to consume the formed •OH. Photocatalytic H_2 production performance on TiO_2 based catalysts was evaluated under visible light irradiation using CH_3OH as scavenger (Table 3). Control experiments indicated that no H_2 is detected in the absence of either irradiation or photocatalyst. Neat TiO_2 shows a very low H_2 production ability (<10 μmol h^{-1}). Although the charge transfer occurred between NiO and TiO_2, leading to a decreased recombination rate of Ni(0.03)Ti as shown in Fig. 7, its photocatalytic activity is still very low because of the poor visible light absorption ability. For R–N(10)Ti, the photocatalytic H_2 production ability increased to 120 μmol h^{-1}, because its lower band gap energy can utilize visible light more effectively. However, high oxygen vacancies concentration on catalyst surface cause the high electrons/holes recombination rate, leading to a decreased decomposition rate of H_2O (Eq. (4)) and less H^+ concentration. Thus, its H_2 production ability is far from our expectation. After depositing only 1 at.% Ni species on TiO_2 with the Ni^0/Ni^{2+} ratio of 0.5, the H_2 production activity of R–Ni(0.01)N(10)Ti increased obviously to 990 μmol h^{-1}. With further increasing Ni species content and Ni^0/Ni^{2+} ratio to 3 at.% and 0.66, the H_2 production rate of R–Ni(0.03)N(10)Ti achieves 1210 μmol h^{-1}, 10 times higher than that of R–N(10)Ti. We propose the possible photocatalytic mechanism is as follows (Fig. 9). Under visible light irradiation, the energy is not sufficient to excite electrons from the valence band to conduction band. Thus neat TiO_2 is inactive. After nitrogen doping, the electron can be excited from the N impurity levels to the conduction band (process A). DFT calculations suggested that the energy level of oxygen vacancy is about 0.8 eV below the bottom of the conduction band [61]. Thus those electrons on conduction band will trap by oxygen vacancies favorably (process B). Those electrons in oxygen vacancies state recombine with the holes in the N impurity levels (process C), leading to a low H_2 production rate of R–N(10)Ti. For R–Ni(*x*)N(*y*)Ti series catalysts, the potential of Ni^{2+}/Ni ($Ni^{2+} + 2e^- = Ni$, −0.23 V) is slightly lower than conduction band (−0.26 V) of anatase TiO_2, meanwhile higher than the reduction potential of H^+/H_2 ($2H^+ + 2e^- = H_2$, 0.00 V) [24]. The photoinduced electrons in the conduction band will transfer to Ni/NiO clusters (process D). These metallic Ni can act as cocatalyst to promote the separation and transfer of photogenerated electrons from conduction band of TiO_2 to Ni/NiO clusters, where reduction of H^+ takes place to produce H_2. Moreover, the valence band

Table 3
Photocatalytic production and quantum yield of prepared TiO_2 based catalysts.

Sample	H_2 (μmol h^{-1})	O_2 (μmol h^{-1})	CO_2 (μmol h^{-1})	Quantum yield (%)
Neat TiO_2	5.5	2.7	–	0.03
Ni(0.03)Ti	8.9	4.5	–	0.05
R–N(10)Ti	110	50	3	0.68
R–Ni(0.01)N(10)Ti	990	481	9.5	6.1
R–Ni(0.03)N(10)Ti	1210	585	13.3	7.5
R–Ni(0.05)N(10)Ti	830	403	8	5.2
Ni(0.03)N(10)Ti	466	225	5.2	2.9
M-Ni(0.03)N(10)Ti	124	56	3.6	0.73

electrons of R–Ni(*x*)N(*y*)Ti series catalysts also can be excited to oxygen vacancies state (process E). Those electrons then transfer from oxygen vacancies state to conduction band by absorbing other photons (process F), finally to Ni/NiO clusters, leading to a more effective visible light utilization. Thus the H_2 production ability improved dramatically. With further increasing the Ni species content, the Ni^0/Ni^{2+} ratio decreases to 0.33, and photocatalytic activity of R–Ni(0.05)N(10)Ti also decreases (830 μmol h^{-1}). This indicates that Ni^0/Ni^{2+} ratio play a significantly important role on the photocatalytic H_2 production ability. Besides, deposition of excessive Ni/NiO clusters leads to the decrease of TiO_2 surface active sites and increase the opacity which decrease the irradiation passing through the reaction suspension solution [62]. For Ni(0.03)N(10)Ti, no metallic Ni exists (Table 2). Thus its H_2 production ability is much lower than that of R–Ni(*x*)N(*y*)Ti series catalysts. The H_2 production ability of M-Ni(0.03)N(10)Ti is only 124 μmol h^{-1}, one tenth of R–Ni(0.03)N(10)Ti. This confirms the intimate heterostructure was formed in R–Ni(*x*)N(*y*)Ti series catalysts which significantly improved the photogenerated charge separation and thereby promoted the photocatalytic efficiency.

The past decade have witnessed the growing interest in photocatalytic water splitting reaction. However, the different light sources with a wide range of intensities and wavelengths, different active surface area, and different reactor geometries, etc. lead to quantitative comparison of hydrogen production rates obtained from different catalysts is meaningless. Therefore, the apparent quantum yield is a more scientific indicator to evaluate the photocatalytic performance of different catalysts. The apparent

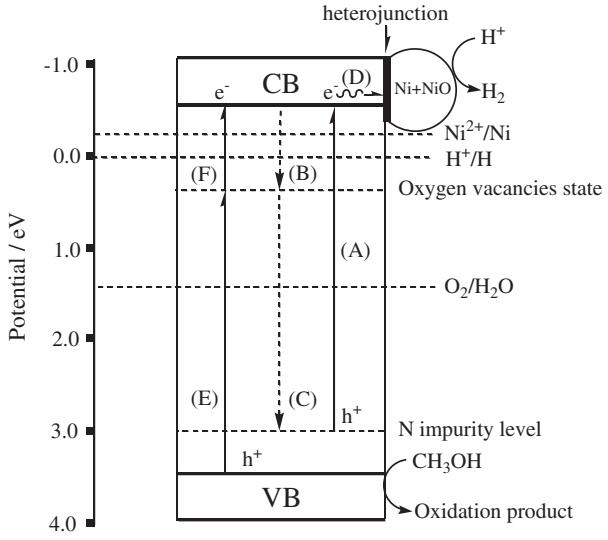

Fig. 9. Mechanism of the charge transfer and photocatalytic H_2 production over R–Ni(*x*)N(*y*)Ti under visible light.

quantum yield of prepared TiO_2 based catalysts was also shown in Table 3. For neat TiO_2 and Ni(0.03)Ti, the apparent quantum yields were very low (<0.1%). However, R–Ni(*x*)N(10)Ti series catalysts exhibited the outstanding apparent quantum yield (higher than 5%). R–Ni(0.03)N(10)Ti exhibited the highest apparent quantum yield, 7.5%. This value is 250 times higher than that of neat TiO_2.

Besides, it is shown in Table 3 that the molar ratio of produced H_2 to O_2 for all the prepared TiO_2 based catalysts were slight lower than 2.0, moreover a small amount of CO_2 was observed. This should be due to that CH_3OH can be oxidized by the formed O_2 molecule to form CO_2 [63], as shown in Eq. (7). Zalas et al. reported that CH_3OH can also undergo photocatalytic reforming to produce H_2 and CO_2 under anaerobic conditions (Eq. (8)) [64]. However, the stoichiometry ratio of consumed O_2 to formed CO_2 was approximatively 1.5:1, which is consistent with that in Eq. (7). Thus the CH_3OH reforming should not occur in this system. Such consuming of O_2 molecule could limit the reverse $H_2+1/2O_2 \rightarrow H_2O$ reaction, and increasing charge separation [63]. [fx2]

$$h^+ + H_2O \longrightarrow H^+ + {}^\bullet OH \quad (4)$$

$$H^+ + e^- \longrightarrow H \quad (5)$$

$$2H \longrightarrow H2 \quad (6)$$

$$CH_3OH + 1.5O_2 \longrightarrow CO_2 + 2H_2O \quad (7)$$

$$CH_3OH + H_2O \rightarrow CO_2 + 3H_2 \quad (8)$$

In order to check the photocatalytic H_2 production stability, the photocatalytic performances of fresh and reused R–Ni(0.03)N(10)Ti were investigated (Fig. 10). The activity of fresh R–Ni(0.03)N(10)Ti keep stable within 20 h, which confirm the photocurrent responses result that R–Ni(0.03)N(10)Ti can provide a stable photocurrent with increasing the illuminated time (Fig. 8). Interestingly, for reused catalyst, the H_2 production ability is lower than 1000 μmol h^{-1} at the beginning 30 min. After that, the activity restores to normal value and keeps stable. Based on above conclusion, we propose that the existing form of Ni species in reused R–Ni(0.03)N(10)Ti is probably changed which cause the decreased activity. Therefore, the XP spectra of reused R–Ni(0.03)N(10)Ti before and after Ar^+ etching is compared and shown in Fig. 11. Before Ar^+ etching, only one peak around 856.6 eV is observed, indicating no metallic Ni exists. However, after Ar^+

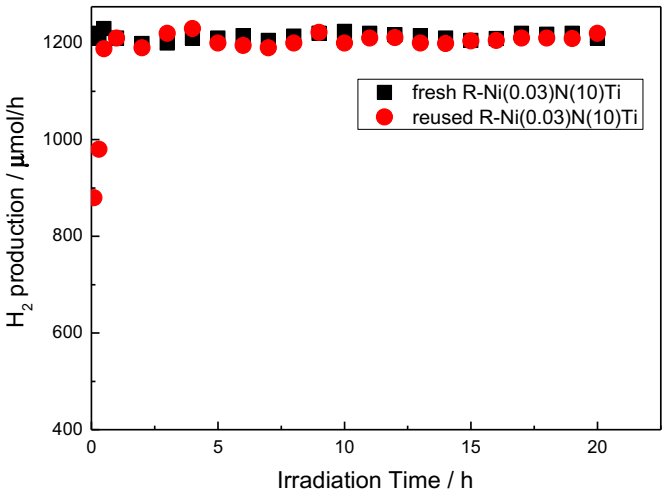

Fig. 10. Photocatalytic H_2 production stability of R–Ni(0.03)N(10)Ti.

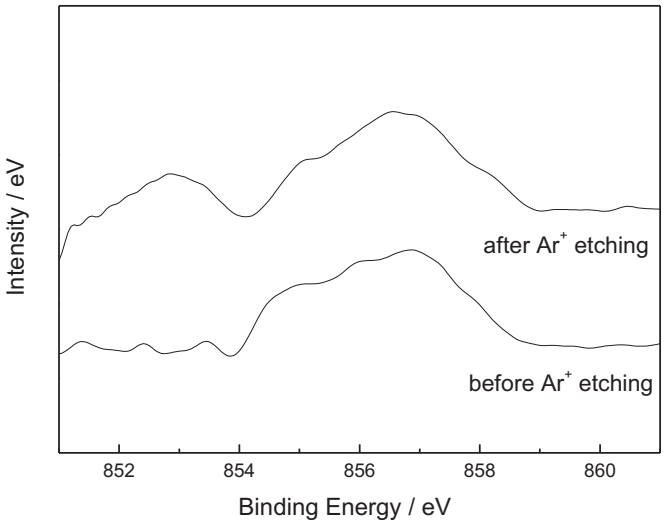

Fig. 11. Comparison of XP spectra of fresh and reused R–Ni(0.03)N(10)Ti.

etching to get rid of the surface layer, metallic Ni located at 852.9 eV appears. This is probably due to that metallic Ni is unstable and easily oxidized to form a NiO thin film in air. Such NiO thin film covers the metallic Ni, which prevents the further oxidation reaction occurred. It is deduced that, at the initial reaction time of reused R–Ni(0.03)N(10)Ti, no metallic Ni is exposed which leads to a lower activity. When the reaction time increases, the photoinduced electrons in the conduction band transfers to NiO clusters and effectively reduces partial Ni^{2+} to Ni^0 atoms, finally exposing Ni clusters [65]. Thus the H_2 production ability of R–Ni(0.03)N(10)Ti restores.

4. Conclusions

A series of visible light responsive Ni/NiO/N–TiO_{2-x} heterojunction nanocomposites were prepared by nonthermal NH_3 plasma treatment. Ni species deposition decreased the surface free energy of nanocomposites, reduced the thermodynamic driving force for particle growth, thus leading to the smaller particle sizes. NH_3 plasma treatment did not influence the crystal structure but shift its absorption edges to the visible light region, reduce partial NiO to metallic Ni, and form high concentration of oxygen vacancies. Charge transfer and structural compensation exists in Ni/NiO/N–TiO_{2-x} nanocomposites, thus stabilize the oxygen vacancy concentrations and cause Ni^{2+} reduction more easily. Ni species are in intimate contact with TiO_2, leading to the formation of heterojunction. Such intimate heterostructure can significantly improve the photogenerated charge separation and thereby promote the photocatalytic efficiency. Ni^0/Ni^{2+} ratio played a significantly important role on the photocatalytic H_2 production ability. Adequate oxygen vacancies concentration could improve the visible light utilization, leading to an enhanced photocatalytic performance. R–Ni(0.03)N(10)Ti exhibited the highest H_2 production ability (1210 μmol h^{-1}) and apparent quantum yield (7.5%), which is 250 times higher than that of neat TiO_2. The H_2 production ability did not decrease for reused Ni/NiO/N–TiO_{2-x} catalyst, indicating its good photocatalytic stability.

Acknowledgment

This work was supported by Program for New Century Excellent Talents in University (No. NCET-11-1011), National Natural Science

Foundation of China (No. 41071317, 30972418, 21103077), National Key Technology R & D Programme of China (No. 2007BAC16B07, 2012ZX07505-001), the Natural Science Foundation of Liaoning Province (No. 20092080).

References

[1] A. Fujishima, K. Honda, Nature 238 (1972) 37–38.
[2] F.E. Osterloh, Chem. Mater. 20 (2008) 35–54.
[3] A. Fujishima, T.N. Rao, D.A. Tryk, J. Photochem. Photobiol. C 1 (2000) 1–21.
[4] S.P. Xu, D.D. Sun, Int. J. Hydrogen Energy 34 (2009) 6096–6104.
[5] R. Dholam, N. Patel, M. Adami, A. Miotello, Int. J. Hydrogen Energy 34 (2009) 5337–5346.
[6] H.J. Wu, Z.H. Zhang, Int. J. Hydrogen Energy 36 (2011) 13481–13487.
[7] X. Zong, H.J. Yan, G.P. Wu, G.J. Ma, F.Y. Wen, L. Wang, C. Li, J. Am. Chem. Soc. 130 (2008) 7176–7177.
[8] W.Q. Fan, Q.H. Lai, Q.H. Zhang, Y. Wang, J. Phys. Chem. C 115 (2011) 10694–10701.
[9] B. Zielinska, E. Borowiak-Palen, R.J. Kalenczuk, Int. J. Hydrogen Energy 33 (2008) 1797–1802.
[10] A. Tanaka, S. Sakaguchi, K. Hashimoto, H. Kominami, ACS Catal. 3 (2013) 79–85.
[11] K. Li, B. Chai, T.Y. Peng, J. Mao, L. Zan, ACS Catal. 3 (2013) 170–177.
[12] S. Sato, Chem. Phys. Lett. 123 (1986) 126–128.
[13] R. Asahi, T. Morikawa, T. Ohwaki, A. Aoki, Y. Taga, Science 293 (2001) 269–271.
[14] A.L. Linsebigler, G. Lu, J.T. Yates Jr., Chem. Rev. 95 (1995) 735–758.
[15] S. Meyer, S. Saborowski, B. Schäfer, ChemPhysChem 7 (2006) 572–574.
[16] M.D. Vasileia, P. Paraskevi, I.K. Dimitris, Chem. Eng. J. 170 (2011) 433–439.
[17] O. Rosseler, M.V. Shankar, M.K. Du, L. Schmidlin, N. Keller, V. Keller, J. Catal. 269 (2010) 179–190.
[18] S. Onsuratoom, S. Chavadej, T. Sreethawong, Int. J. Hydrogen Energy 36 (2011) 5246–5261.
[19] X.M. Wu, Q.Q. Song, L.S. Jia, Q.B. Li, C. Yang, L.Q. Lin, Int. J. Hydrogen Energy 37 (2012) 109–114.
[20] R. Brahimi, Y. Bessekhouad, A. Bouguelia, M. Trari, J. Photochem. Photobiol. A 186 (2007) 242–247.
[21] J.S. Jang, S.J. Hong, J.Y. Kim, J.S. Lee, Chem. Phys. Lett. 475 (2009) 78–81.
[22] C.J. Chen, C.H. Liao, K.C. Hsu, Y.T. Wu, J.C.S. Wu, Catal. Commun. 12 (2011) 1307–1310.
[23] S. Oros-Ruiz, R. Zanella, B. Prado, J. Hazard. Mater. (2013), http://dx.doi.org/10.1016/j.jhazmat.2013.04.010.
[24] J.G. Yu, Y. Hai, B. Cheng, J. Phys, Chem. C 115 (2011) 4953–4958.
[25] R.H. Zhang, Q. Wang, J. Liang, Q. Li, J.F. Dai, W.X. Li, Physica B 407 (2012) 2709–2715.
[26] X. Zhang, Q.Q. Liu, Appl. Surf. Sci. 254 (2008) 4780–4785.
[27] S.Z. Hu, F.Y. Li, Z.P. Fan, Bull. Korean Chem. Soc. 33 (2012) 4052–4058.
[28] Z.L. Jin, X.J. Zhang, Y.X. Li, S.B. Li, G.X. Lu, Catal. Commun. 8 (2007) 1267–1273.
[29] H. Kato, A. Kudo, J. Phys. Chem. B 105 (2001) 4285–4292.
[30] X.Z. Shen, Z.C. Liu, S.M. Xie, J. Guo, J. Hazard, Mater 162 (2009) 1193–1198.
[31] M. Kang, J. Mol. Catal. A Chem. 197 (2003) 173–183.
[32] L. Pan, J.J. Zou, X.W. Zhang, L. Wang, Ind. Eng. Chem. Res. 49 (2010) 8526–8531.
[33] J.G. Yu, G.H. Wang, B. Cheng, M.H. Zhou, Appl. Catal. B 69 (2007) 171–180.
[34] M. Anpo, M. Takeuchi, J. Catal. 216 (2003) 505–516.
[35] S.W. Liu, J.G. Yu, M. Jaroniec, J. Am. Chem. Soc. 132 (2010) 11914–11916.
[36] H. Irie, S. Miura, K. Kamiya, K. Hashimoto, Chem. Phys. Lett. 457 (2008) 202–205.
[37] H. Ozaki, N. Fujimoto, S. Iwamoto, M. Inoue, Appl. Catal. B 70 (2007) 431–436.
[38] H. Abe, T. Kimitani, M. Naito, J. Photochem. Photobiol. A 183 (2006) 171–175.
[39] X. Qiu, M. Miyauchi, H. Yu, H. Irie, K. Hashimoto, J. Am. Chem. Soc. 132 (2010) 15259–15267.
[40] J.G. Yu, X.J. Zhao, Q.N. Zhao, Mater. Chem. Phys. 69 (1–3) (2001) 25–29.
[41] B.P. Payne, M.C. Biesinger, N.S. McIntyre, J. Electron Spectrosc. Relat. Phenom. 175 (2009) 55–65.
[42] K. Yamada, H. Yamane, S. Matsushima, H. Nakamura, K. Ohira, M. Kouya, K. Kumada, Thin Solid Films 516 (2008) 7482–7487.
[43] K. Yamada, H. Yamane, S. Matsushima, H. Nakamura, T. Sonoda, S. Miura, K. Kumada, Thin Solid Films 516 (2008) 7560–7564.
[44] H.X. Li, J.X. Li, Y.N. Huo, J. Phys. Chem. B 110 (2006) 1559–1565.
[45] W.W. Lin, H.Y. Cheng, L.M. He, Y.C. Yu, F.Y. Zhao, J. Catal. 303 (2013) 110–116.
[46] C.C. Xu, J.W. Zondlo, M.Y. Gong, X.B. Liu, J. Power Sources 196 (2011) 116–125.
[47] K.S. Abdel-Halim, M.H. Khedr, M.I. Nasr, M.Sh Abdel-wahab, J. Alloy. Compd. 463 (2008) 585–590.
[48] M. Bahgat, M.K. Paek, J.J. Pak, J. Alloy. Compd. 472 (2009) 314–318.
[49] Y.W. Zhang, W.Z. Ding, S.Q. Guo, K.D. Xu, Chin. J. Nonferrous Met. 14 (2004) 317–321.
[50] B.S. Liu, L.P. Wen, X.J. Zhao, Sol. Energy Mater. Sol. Cells 92 (2008) 1–10.
[51] Q.P. Wu, Q. Zheng, R. Krol, J. Phys. Chem. C 116 (2012) 7219–7226.
[52] R. Long, N.J. English, Chem. Mater. 22 (2010) 1616–1623.
[53] X.G. Ma, Y. Wu, Y.H. Lu, J. Xu, Y.J. Wang, Y.F. Zhu, J. Phys. Chem. C 115 (2011) 16963–16969.
[54] H. Nakajima, T. Mori, Q. Shen, T. Toyoda, Chem. Phys. Lett. 409 (2005) 81–84.
[55] F. Dong, W.R. . Zhao, Z.B. Wu, S. Guo, J. Hazard. Mater. 162 (2009) 763–770.
[56] Z.Y. Jiang, Q. Kuang, Z.X. Xie, L.S. Zheng, Adv. Funct. Mater. 20 (2010) 3634–3645.
[57] B.L. He, B. Dong, H.L. Li, Electrochem. Commun. 9 (2007) 425–430.
[58] Q.W. Huang, S.Q. Tian, D.W. Zeng, X.X. Wang, W.L. Song, Y.Y. Li, W. Xiao, C.S. Xie, ACS Catal. 3 (2013) 1477–1485.
[59] Z.R. Hesabi, N.K. Allam, K. Dahmen, H. Garmestani, M.A. El-Sayed, ACS Appl. Mater. Interf. 3 (2011) 952–955.
[60] Y. Liu, Y.X. Yu, W.D. Zhang, J. Phys. Chem. C 117 (2013) 12949–12957.
[61] S. Livraghi, M.C. Paganini, E. Giamello, A. Selloni, C. Di Valentin, G. Pacchioni, J. Am. Chem. Soc. 128 (2007) 15666–15671.
[62] J.G. Yu, X.J. Zhao, Q.N. Zhao, Thin Solid Films 379 (2000) 7–14.
[63] A. Iwase, H. Kato, A. Kudo, Catal. Lett. 108 (2006) 7–10.
[64] M. Zalas, M. Laniecki, Sol. Energ. Mat. Sol. C. 89 (2005) 287–296.
[65] A.J. Bard, R. Parsons, J. Jordan, in: Marcel Dekker (Ed.), Standard Potentials in Aqueous Solution, 1985. New York.